High Efficiency PMSM With High Slot Fill Factor Coil for Heavy-Duty EV Traction Considering AC Resistance

Jun-Woo Chin, Kyoung-Soo Cha, Min-Ro Park, Soo-Hwan Park, Eui-Chun Lee, and Myung-Seop Lim, *Member, IEEE*

***Abstract*—Electric vehicle (EV) systems require a high energy-efficiency traction motor so that the motors for EV traction should achieve high efficiency and power density. Hence, a permanent magnet synchronous motor (PMSM) for EV traction using a maximum slot occupation (MSO) coil has been investigated in this study. By applying the MSO coil, high torque density was achieved, but an additional loss, which decreases the efficiency, was incurred through alternating current (AC) resistance. To reduce the AC resistance of the MSO coil, the following process was performed: First, by investigation using the analytical method, pole/slot numbers, current density and number of parallel circuits affecting the frequency, the shape and number of conductors were chosen as important variables. Resistances of the MSO coil with a stator core were analyzed according to the chosen variables above. From the results, MSO coil applied PMSM with proper pole/slot numbers, current density, and parallel circuits was determined to improve the efficiencies at the base and maximum speeds. To accurately estimate the efficiency of the determined model, loss evaluation methods were explained. Subsequently, the determined MSO coil applied model was compared with the conventional model having round wires, and the improvements were verified by load testing.**

***Index Terms*—AC resistance, current density, efficiency, EV traction, fill factor, loss, maximum slot occupation (MSO) coil, parallel circuit, PMSM, pole/slot number.**

I. Introduction

CURRENTLY, the electric machine industry expends considerable effort on higher efficiency and power density required for increasing energy efficiency [1]–[3]. Especially for electric vehicle (EV) traction systems, requiring a wide driving range and various driving cycles, challenges remain to enhance the efficiency at both low and high speeds [4]. To achieve such goals, significant research on electrical machine needs to be conducted extensively, especially for the motor.

To improve motor power and torque densities, various winding types have been studied to increase the slot fill factor. An example is the hairpin winding, a rectangular wire type, whose fill factor can attain 60%, compared to the conventional round wire, attaining nearly 40%. Such an improvement enhances the torque density but also increases the alternating current (AC) resistance due to the larger conductor area. The phenomenon known as AC resistance occurs by eddy current when the AC flows through the conductor in a slot surrounded by the stator core. The AC resistance of hairpin windings for automotive applications is studied, and designs were proposed [5], [6]. There has also been research conducted related to the design of high-power density and high-efficiency motors applying hairpin windings [7].

From an efficiency viewpoint, there are several studies on reducing losses such as studying new core structures, control strategies, winding connections [8]–[10], and manufacturing methods [11]. Moreover, investigations into AC resistance of motors, using analytical and numerical methods were performed [12], [13]. However, there is little work about designing motors that consider additional copper loss due to AC resistance [14], [15].

In this study, a high-efficiency permanent magnet synchronous motor (PMSM) for EV traction was investigated using the maximum slot occupation (MSO) coil, which has a high slot fill factor. Before analyzing the AC resistance of the MSO coil, the MSO coil characteristics were first inspected. Using the analytical method, the parameters such as frequency, conductor height, and number of conductor layers affecting the AC resistance of the MSO coil were then investigated. Second, based on the analyzed parameters, the PMSM variables affecting AC resistance were chosen by considering their tendencies for PMSM with an MSO coil under both of base and maximum speeds. Finally, a PMSM for EV traction using an MSO coil was proposed by selecting the appropriate pole/slot numbers, current density, and parallel circuits, which are the chosen variables for the AC resistance reduction and efficiency improvement.

Manuscript received February 12, 2020; revised June 5, 2020 and October 13, 2020; accepted October 28, 2020. Date of publication November 2, 2020; date of current version May 21, 2021. This work was supported by the National Research Foundation of Korea (NRF) grant funded by the Korea government (MSIT) (NRF-2020R1A4A4079701). Paper no. TEC-00147-2020. *(Corresponding author: Myung-Seop Lim.)*

Jun-Woo Chin, Kyoung-Soo Cha, Soo-Hwan Park, and Myung-Seop Lim are with the Department of Automotive Engineering, Hanyang University, Seoul 04763, South Korea (e-mail: cjw1254@hanyang.ac.kr; chakungsoo@hanyang.ac.kr; shwanp14@hanyang.ac.kr; myungseop@hanyang.ac.kr).

Min-Ro Park is with the Interactive Robotics R&D Division, Korea Institute of Robotics & Technology Convergence, Pohang 37553, South Korea (e-mail: minro@kiro.re.kr).

Eui-Chun Lee is with the Department of Automotive Engineering, Hanyang University, Seoul 04763, South Korea, and also with the Korea Institute of Industrial Technology, Daegu 330-32, South Korea (e-mail: 2chun@kitech.re.kr).

Color versions of one or more of the figures in this article are available online at https://ieeexplore.ieee.org.

Digital Object Identifier 10.1109/TEC.2020.3035165

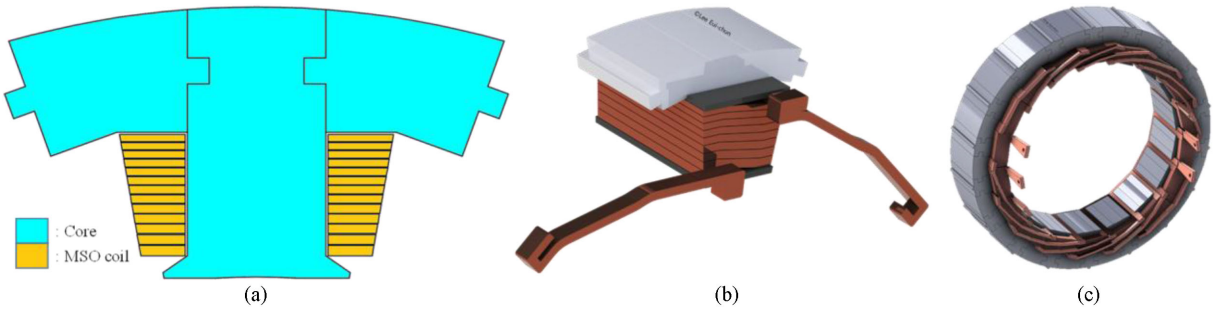

Fig. 1. Structure of MSO coil. (a) 2-D cross-section. (b) Assembly for one pair of MSO coil and stator cores. (c) Complete stator assembly.

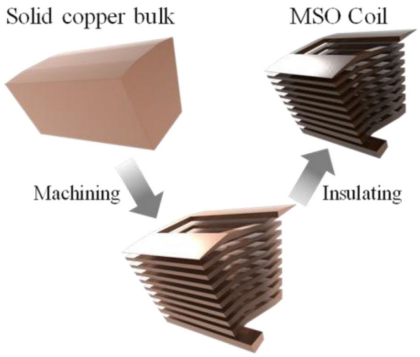

Fig. 2. Manufacturing process of MSO coil.

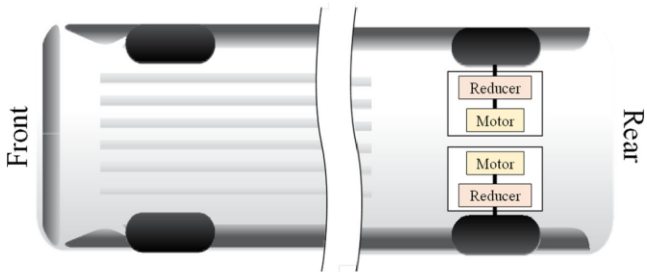

Fig. 3. Diagram of power system configuration for an electric bus.

The results were compared with the model using round wire and were verified by the test.

II. Characteristics of MSO Coil

The MSO coil is an advanced winding technology invented by the Korea Institute of Industrial Technology (KITECH), in which the fill factor of a conductor can be up to 80%. The MSO coil structure and its assembly with the core are presented in Fig. 1. The cross-section of the MSO coil and core for one tooth is shown in Fig. 1(a). Also, Fig. 1(b) presents the assembly of the MSO coil, slot liner, and core for one tooth, and Fig. 1(c) shows a total stator core assembly using an MSO coil.

The manufacturing process of an MSO coil is briefly presented in Fig. 2 [16]. With a device for manufacturing the MSO coil, the shape of an MSO coil is first machined from a solid copper bulk. To avoid current flowing between the conductor turns in the MSO coil, Teflon and Polyimide insulation is used. After insulation, the MSO coil is assembled with a separate core, as shown in Fig. 1.

The advantages of applying the MSO coil are as follows:

1) It can reduce the resistance and current density of the coil, increasing the area of conductors by maximizing the conductor fill factor to 80%, leading to a more flexible motor design.
2) The heat dissipation is improved by increasing the contact area between the coil and core compared to other winding technologies.

The disadvantages of the MSO coil are as follows:

1) Due to the conductor shape as shown in Fig. 1(a), the AC resistance (generated by the eddy current) is critical when the system frequency increases, resulting in lower efficiency.
2) Based on the AC resistance mentioned above, additional copper losses can lead to serious high-temperature problems, such as burning.
3) Only applicable to concentrated winding.

Thus, although the increased fill factor provides design flexibility with an MSO coil, it is essential to analyze parameters that affect AC resistance before designing a traction motor.

III. AC Resistance of MSO Coil

When the AC flows through the conductor in a slot surrounded by the stator core, an eddy current is generated by the slot leakage flux in the conductors, changing the current density distribution and increasing resistance. This phenomenon is an effect of the increased resistance, defined as AC resistance.

Before designing a high-efficiency traction motor, the AC resistance in the MSO coil, discussed in this section, is assessed through an analytical method. First, the analytic method is obtained by modifying the existing equation for a rectangular wire. Subsequently, the parameters that have significant effects on AC resistance of the MSO coil are identified, and its DC and AC resistances are analyzed according to design variables such as pole/slot number, current density, and number of parallel circuits.

The motor proposed in this manuscript is a traction motor for an electric bus (EBUS), which is a heavy-duty vehicle as shown in Fig. 3. From the vehicle specifications shown in Table I, the driving cycle of a heavy-duty urban dynamometer driving schedule (HDUDDS), and vehicle dynamics, the required maximum torque, the base and maximum speeds of the traction motor are derived as shown in Fig. 4. The base and maximum speeds

TABLE I
SPECIFICATION OF TARGET VEHICLE

Item	Unit	Value
Curb Weight	kg	12500
Frontal Area	m^2	6.72
Wheel Radius	m	0.48
Gear Ratio	-	9.5
Gear Efficiency	%	95
Aerodynamic Drag Coefficient	-	0.7
Rolling Resistance Coefficient	-	0.07
Number of Passengers	-	40
Weight per Passenger	kg	60

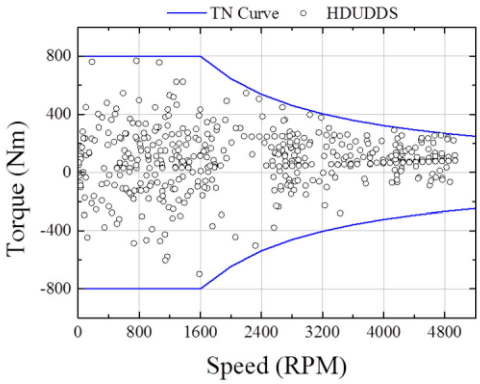

Fig. 4. Operating traction motor points for the target vehicle.

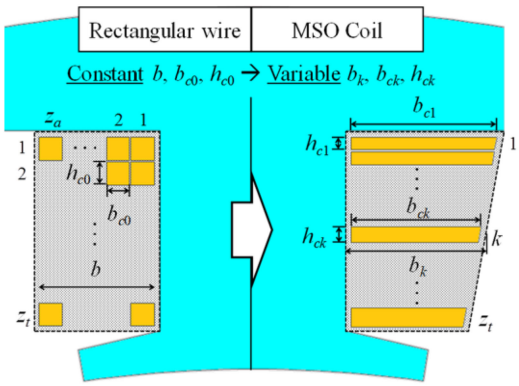

Fig. 5. Conductors in slot.

of the traction motor presented in this paper are lower than those of a traction motor for a light-duty vehicle [17]–[19]. As such, when analyzing the AC resistance of the MSO coil, the base and maximum speeds of 1600 RPM and 5200 RPM are adopted.

A. Proposed Analytical Method

Many researchers have studied AC resistance of the coil. In particular, Pyrhönen studied an analytical approach for determining the AC resistance of a series-connected rectangular wire, as shown in Fig. 5 [20]. A differential equation describing the above phenomena is derived by applying Ampere's and Faraday's laws on the conductors in the slot and is solved by applying boundary conditions; the results are shown as the existing equation in the left side of Table II.

However, the existing equation has some limitations during real-world application of the actual PMSM stator and the MSO coil: The existing method assumes that the slot has the same width (b) along the row direction, but the actual stator core slot has varying width (b_k) as seen in Fig. 5. Furthermore, the conductors in the slot have the same height (h_{c0}) and width (b_{c0}) along the row and column as shown in the left side of Fig. 5, while in the actual MSO coil, they vary along the row direction. To overcome the above limitations, the proposed method adopted varying MSO coil height (h_{ck}) and width (b_{ck}), and varying slot width (b_k), as shown in the right side of Fig. 5. By modifying the existing equation, a method for calculating the AC resistance of the MSO coil is proposed as (1)–(4) in Table II. Through the proposed analytical method, parameters such as frequency, conductor height, and number of conductor layers are identified as important parameters that affect the AC resistance of the MSO coil. Then, the PMSM variables related to those parameters are derived in the following section.

B. Determination of Variables Considering AC Resistance of MSO Coil

First, when the rotational speed of the traction motor is decided, the frequency depends on the number of poles. The effect of the number of poles influencing the conductor layers in the slot while the series turns per phase are constant. In addition, the shape of the conductor (specifically the cross-sectional area, width, and height) is determined by the current density and number of parallel circuits. Hence, using the proposed analytical method, the effect on the AC resistance of the MSO coil is analyzed in this section according to the aforementioned variables such as the number of poles, the current density, and the number of parallel circuits.

When analyzing the AC resistance trend according to variables, the conditions are as follows:

1) The number ratio of poles to slots is 2:3, which is widely used in traction motors for HEV/EV [21], [22].
2) The back electromagnetic force is assumed to be the same due to the constant series turns per phase.
3) Series turns per phase of the armature winding are 36, which is applicable to pole/slot numbers of 8/12, 12/18, and 16/24.
4) The MSO coil slot fill factor is 80%.
5) The base and maximum speeds are 1600 and 5200 RPM, respectively.
6) The cross-sectional area of each conductor in one slot with the same pole/slot numbers, current density, and parallel circuit is equal.
7) The end coil resistance is considered as DC resistance only.
8) The core nonlinearity is ignored in this section.

When investigating the AC resistance of an MSO coil according to pole/slot numbers, current density, and number of parallel circuits with the analytical method in Section III, the

TABLE II
ANALYTICAL METHOD FOR CALCULATING AC RESISTANCE

Contents	Existing equation (Rectangular wire, proposed by J. Pyrhönen [20])	Proposed method (MSO Coil)	
Reduced conductor height	$\xi = h_{c0}\sqrt{\pi f \mu_0 \sigma_c z_a b_{c0} / b}$	$\xi_k = h_{ck}\sqrt{\pi f \mu_0 \sigma_c b_{ck} / b_k}$	(1)
Resistance factor of k^{th} layer (k_{Rk})	$k_{Rk} = \varphi(\xi) + k(k-1)\psi(\xi)$ $\left(\varphi(\xi) = \xi\frac{\sinh 2\xi + \sin 2\xi}{\cosh 2\xi - \cos 2\xi},\ \psi(\xi) = 2\xi\frac{\sinh \xi - \sin \xi}{\cosh \xi + \cos \xi}\right)$	$k_{Rk} = \varphi(\xi_k) + k(k-1)\psi(\xi_k)$ $\left(\varphi(\xi_k) = \xi_k\frac{\sinh 2\xi_k + \sin 2\xi_k}{\cosh 2\xi_k - \cos 2\xi_k},\ \psi(\xi_k) = 2\xi_k\frac{\sinh \xi_k - \sin \xi_k}{\cosh \xi_k + \cos \xi_k}\right)$	(2)
Resistance factor (k_R)	$k_R = R_{total} / R_{DC} = \frac{1}{z_t}\sum_{k=1}^{z_t} k_{Rk} = \varphi(\xi) + \frac{(z_t^2 - 1)}{3}\psi(\xi)$	$k_R = R_{total} / R_{DC} = \frac{1}{z_t}\sum_{k=1}^{z_t} k_{Rk}$	(3)
Total resistance considering AC resistance (R_{total})	$R_{total} = k_R R_{DC}$	$R_{total} = k_R R_{DC}$	(4)

other variables except the variables shown, are independent variables, and each variable only affects the parameters such as the frequency, shape of the conductor, and number of conductor layers. For example, the frequency, number of conductor layers, and shape of conductors vary when the pole/slot number changes; however, only the shape of conductors varies when the current density changes. Additionally, the number of conductor layers and the shape of conductors vary as the number of parallel circuits changes.

The reasons for the pole/slot combination being selected as 2:3 are offered based on the references. It is apparent that an MSO coil cannot be applied to the distributed winding combination of poles and slots. Therefore, only concentrated winding, especially for tooth-coil winding are taken into account for the combination of poles and slots. Even if the majority of the concentrated and tooth-coil windings are fractional slot windings, critical differences exist depending on whether the pole/slot combination includes subharmonics or not. The effect of subharmonics on PMSM can be divided into two parts:

1) Increasing rotor loss [23]–[25].
2) Generating a low spatial harmonic order of the radial force which induces significant vibration [26], [27].

This study focuses on reducing losses and enhancing PMSM efficiency for EV traction. Therefore, increasing rotor loss can be critical. Furthermore, the noise, vibration, and harness characteristics are also important in EV traction application. As a result, the combination of the number of poles and slots with a 2:3 ratio is considered in this study.

Following the above conditions, analysis models according to the pole/slot numbers are shown in Fig. 6. Assuming the constant series turns per phase and parallel circuit as two, the series turns per coil decrease when the number of poles increases. Fig. 7 shows the DC and AC resistances according to the number of poles. From the assumption that the cross-sectional area of each conductor in one slot at the same pole/slot numbers, current density, and parallel circuit is equal, the coil-side DC resistance is taken as constant with the varying pole/slot numbers. However, the end-coil DC resistance decreases because the end coil length becomes shorter when the pole/slot numbers increase, as shown in Fig. 7. In contrast, Fig. 7(a) and (b) show that the AC resistance affects higher pole/slot numbers (as they have a higher

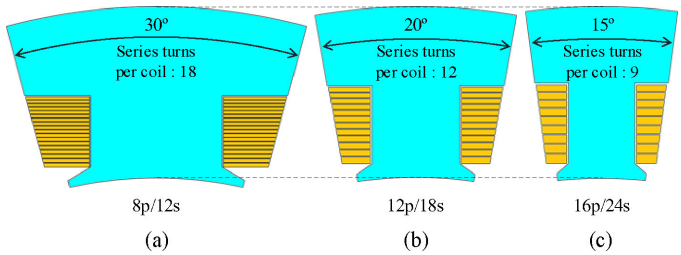

Fig. 6. MSO Coil with stator core according to pole/slot numbers. (a) 8p/12s. (b) 12p/18s. (c) 16p/24s.

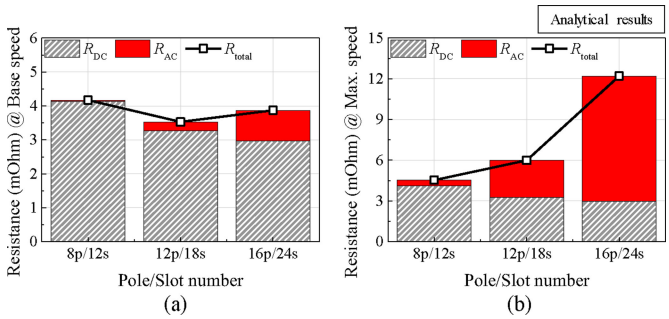

Fig. 7. Resistances of MSO Coil according to number of pole/slot numbers (Analytical results). (a) Base speed. (b) Maximum speed.

frequency), larger cross-sectional area and conductor height, as shown in Fig. 6(b) and (c). In particular, the AC resistance is clearly identified as high value in the maximum speed shown in Fig. 7(b).

Next, resistance trends according to current density are analyzed. As mentioned, the cross-sectional area, height, and width of the conductor decrease as the current density increases as shown in Fig. 8(a). Therefore, the DC resistance of MSO coil increases along with the current density. However, with higher current density, AC resistance also has a lower effect because conductors have a smaller cross-sectional area, height, and width. This trend increases with the higher speed (frequency), as shown in Fig. 9.

Last, resistance trends according to the number of parallel circuits are analyzed based on the analysis model in Fig. 8(b).

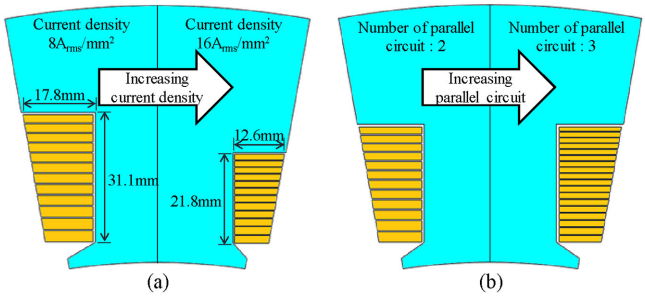

Fig. 8. MSO Coil with stator core according to variables. (a) Current density. (b) Parallel circuits.

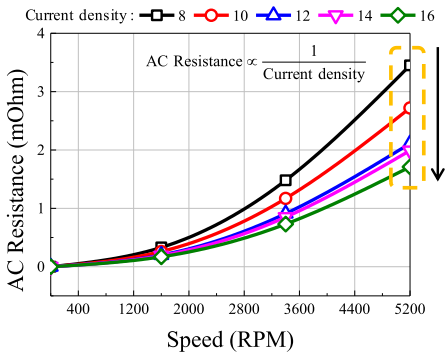

Fig. 9. AC resistances of MSO Coil according to current density with varying speed (Analytical results).

When the number of parallel circuits vary, the DC resistance is the same. Otherwise, Fig. 8(b) shows increasing turns per coil and decreasing cross-sectional area and conductor height with an increasing number of parallel circuits, resulting in a decrease of AC resistance shown in Fig. 10. The higher the number of parallel circuits, the more advantageous it is in terms of AC resistance.

As a result, the pole/slot number, current density, and number of parallel circuits were selected as PMSM variables for EV traction which critically affect AC resistance.

IV. Traction Motor Considering AC Resistance of MSO Coil

The MSO coil analysis considering AC resistance, becomes important when using the MSO coil in a high-efficiency EV traction motor. The previous study determined the PMSM variables using an analytical method. A finite element analysis (FEA) is therefore conducted to consider the core nonlinearity when delineating an EV traction motor using the MSO coil. First, the design specification of a conventional model with round wire, which will be compared with MSO coil model, is introduced. Table III shows PMSM specifications for EV traction and Table IV summarizes the information related to the conventional model with round wire. Next, the AC resistance of the MSO coil applied traction motor with varying pole/slot numbers and current densities are analyzed. Previously, the number of parallel circuits was determined as two, because the

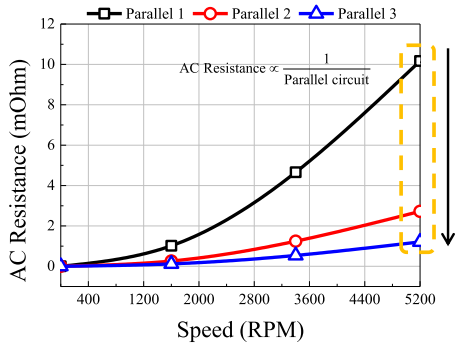

Fig. 10. AC Resistances of MSO Coil according to number of parallel circuits with varying speed (Analytical results).

TABLE III
Specifications of PMSM for EV Traction

Contents	Unit	Value
DC link voltage	V_{DC}	360
Line current limit	A_{rms}	500
Output power	kW	135
Maximum torque	Nm	800
Base speed	RPM	1600
Maximum speed	RPM	5200

TABLE IV
Information about Conventional Model With Round Wire

Contents	Unit	Value
Pole / Slot	-	12 / 18
Current density	A_{rms}/mm^2	11
Series turns per phase	-	39
Slot fill factor	%	40
Number of parallel circuits	-	2
Stator diameter / Stack length	mm	445 / 85
Core material	-	27PNX1350F
PM residual induction	T	1.204 (@100°C)

minimum MSO coil conductor height ($h_{\min.}$) should be no less than 1.5 mm due to its manufacture. Using the MSO coil features, the PMSM analysis is performed with a slot fill factor of 80%. Subsequently, evaluation methods of losses and thermal analysis are presented to accurately estimate the motor efficiency.

A. Determination of Pole/Slot Number

Considering the pole to slot ratio as 2:3, pole/slot numbers from 8/12 to 16/24 are analyzed and their shape can be seen in Fig. 6. Considering the core nonlinearity, the amplitude and phase angle are 480 A_{rms} and 10°, and 270 A_{rms} and 70°, for base and maximum speeds, respectively.

Fig. 11 shows the simulation results of resistances according to number of poles and slots. Except for core nonlinearity, the analysis condition for the FEA is the same as the condition in Section. III. B. The simulation results show a tendency similar to the analytical method results proposed in Fig. 7 for the same reason as that presented in Section III. B. At the base speed

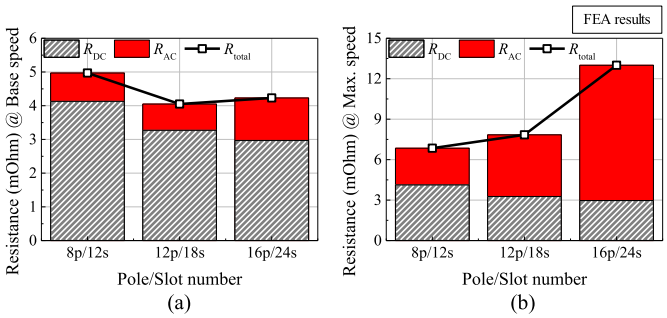

Fig. 11. Resistances of MSO Coil according to pole/slot numbers (FEA results). (a) Base speed. (b) Maximum speed.

shown in Fig. 11(a), the pole/slot number of 12/18 shows the lowest resistance compared to other pole/slot combinations. At the maximum speed shown in Fig. 11(b), a pole/slot combination of 8/12 represents the lowest resistance. Consequently, among the pole/slot numbers, 12/18 was chosen, having the lowest resistance at base speeds, and not lowest but considerably low resistance at maximum speeds. Afterwards, the rotor of the conventional model is shared with the designed model because the pole/slot number is the same as the convention model.

B. Determination of Current Density

After the rotor shape specification, the series turns per phase was selected as 39, satisfying the output at base speed and considering the inverter DC link voltage of 360 V_{DC}. Voltage and current were obtained from the *d-q* axis voltage equation, applying a control strategy of maximum torque per ampere (MTPA). Circuit parameters of the voltage equation, such as flux linkage and *d-q* axis inductances were obtained through FEA [28]–[30]. With a series turns per phase of armature winding as 39, the output torque, resistances, and copper losses according to current densities from 8 to 14 A_{rms}/mm^2 were analyzed.

Fig. 12 shows the tendency of shape, torque, and copper losses according to the current density. The split ratio increases as the current density increases because the stator outer diameter decreases as shown in Fig. 12(a). From the analyzed results, the PMSM with the MSO coil was set at a current density of 11 A_{rms}/mm^2, with minimum copper losses at maximum speed while satisfying the torque requirement at base speed and the conductor minimum thickness ($h_{min.}$) of 1.5 mm as shown in Fig. 12(b) and (c). Moreover, the FEA results of Fig. 13, representing resistance according to current density, have a similar trend to results using the analytical method, as shown in Fig. 9.

C. Loss Evaluation

So far, this study focused on the copper losses considering AC resistance. To precisely estimate the PMSM efficiency, evaluation methods for losses, such as mechanical and iron losses, are required and presented in this section.

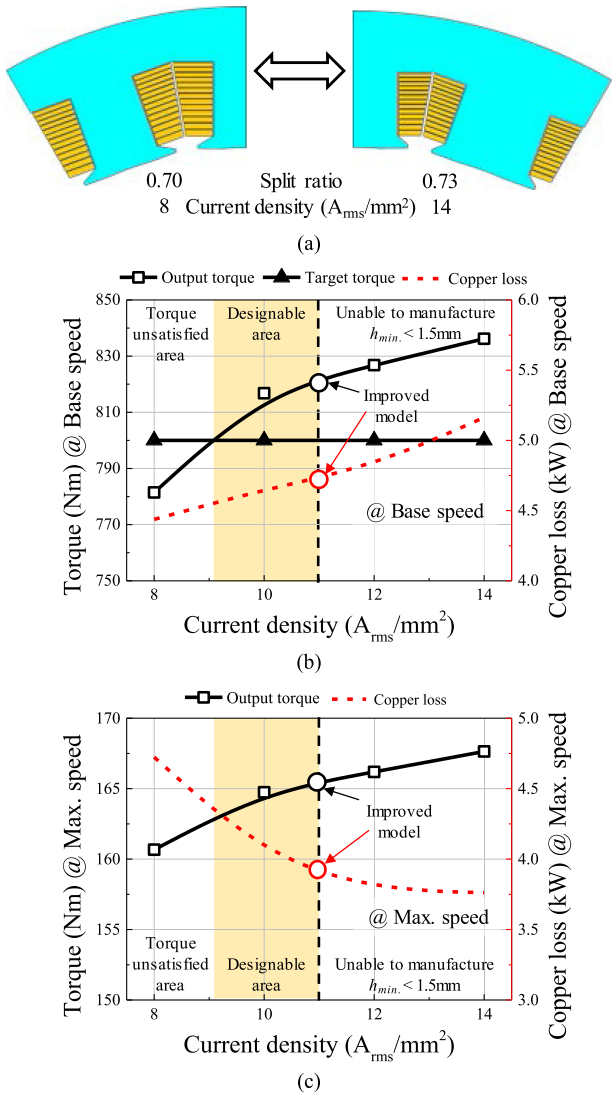

Fig. 12. Tendency of shape, torque and copper loss according to current density (FEA results). (a) Shape of stator. (b) Base speed. (c) Maximum speed.

1) Iron Loss: When there are time-varying fluxes flowing through the core, iron loss occurs, and its accurate evaluation is important to calculate the traction motor characteristics and efficiency [31]. Fig. 14 shows the calculation process of the iron loss through FEA. The harmonics in the magnetic flux density in radial and tangential components are considered up to the 30th order. The process is described as follows:

Step 1: Magnetic flux density waveforms of each element for one period of electrical angle are calculated using two-dimensional FEA considering nonlinearity.

Step 2: By harmonic analysis, the obtained magnetic flux density is compartmentalized into the harmonic order with magnitude.

Step 3: With the iron loss data according to frequency and magnetic flux density from the manufacturer, the corresponding iron losses are determined.

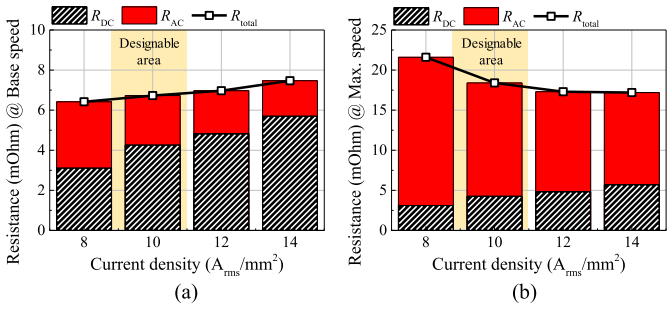

Fig. 13. Resistances of MSO Coil according to current density (FEA results). (a) Base speed. (b) Maximum speed.

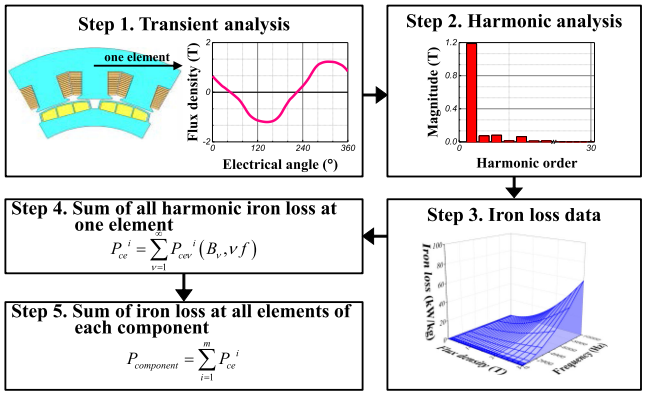

Fig. 14. Process of iron loss calculation.

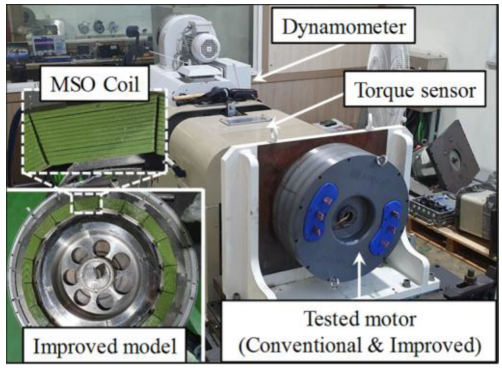

Fig. 15. Test setup for no-load and load test.

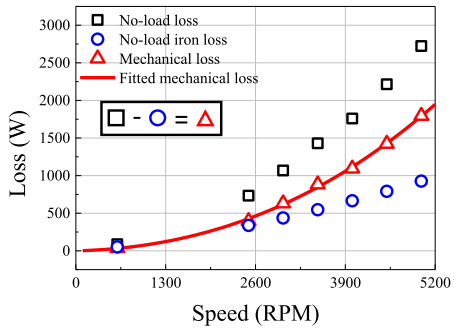

Fig. 16. Test and fitted result of mechanical loss.

Step 4: The iron losses of all harmonic orders are summed in each element.

Step 5: The iron losses of all elements are added to calculate the total motor iron loss.

Based on the above process, the iron loss is mapped according to the amplitude and phase angle of current and speed.

2) Mechanical Loss: When the motor rotates, a mechanical loss is generated due to the mechanical friction torque, composed of bearing and windage frictions. As the bearing supports the weight of the rotor, the friction generated due to the applied load is constant. In addition, the bearing friction is also caused by viscosity. The lubricant that allows the smooth roll of rolling elements, causes viscous bearing friction, which varies with PMSM rotational speed [32]–[34]. Furthermore, the windage friction occurs between the rotor and the stator owing to the shear stress of the air. Regarding aerodynamics, this stress produces windage friction torque proportional to the quadratic term of the angular velocity [31]. Therefore, the friction torque and mechanical loss can be expressed as (5) and (6), respectively,

$$\begin{aligned} T_{\text{friction}} &= T_{\text{appliedload}} + T_{\text{viscosity}} + T_{\text{windage}} \\ &= a_0 + a_1\omega_{\text{m}}^{2/3} + a_2\omega_{\text{m}}^2 \end{aligned} \tag{5}$$

$$\begin{aligned} P_{mechanical} &= T_{\text{friction}}\omega_{\text{m}} = a_0\omega_m + a_1\omega_{\text{m}}^{5/3} + a_2\omega_{\text{m}}^3 \\ &= 0.195\omega_{\text{m}} + 4.853 \times 10^{-3}\omega_{\text{m}}^{5/3} \\ &\quad + 2.495 \times 10^{-6}\omega_{\text{m}}^3 \end{aligned} \tag{6}$$

where ω_{m} is the angular velocity. The coefficients a_0, a_1, and a_2 can be obtained from the mechanical loss test results as follows.

Due to the abovementioned complexity, it is difficult to estimate the mechanical loss by analytical or numerical methods. In Section IV. A, both the improved and conventional models have the same rotor shape. Therefore, the mechanical loss is reflected through data fitting based on the measured mechanical loss of the conventional model. The experimental set up for the no-load torque test is shown in Fig. 15; however, the improved model is replaced with the conventional model. When the dynamometer rotates the motor under no-load, the measured no-load loss indicates the sum of the no-load iron and the mechanical losses. Consequently, the mechanical loss is calculated by subtracting the no-load iron loss from the total no-load loss. The no-load iron loss was obtained via nonlinear FEA presented in the previous section. Fig. 16 shows the examined losses and the mechanical loss as the no-load test results. From the tested mechanical loss, coefficients a_0, a_1, and a_2 were obtained by the least square method. The fitted mechanical loss for all speed ranges was used when evaluating loss.

D. Thermal Consideration

The conventional round wire has a circular shape so that each conductor contact in line or point which is very small touching area. Moreover, when the heat transfer occurs between coil of round wire and stator core, the same phenomenon abovementioned takes place and it results in degradation of heat dissipation rate. Furthermore, the slot fill factor of round wire coil is low

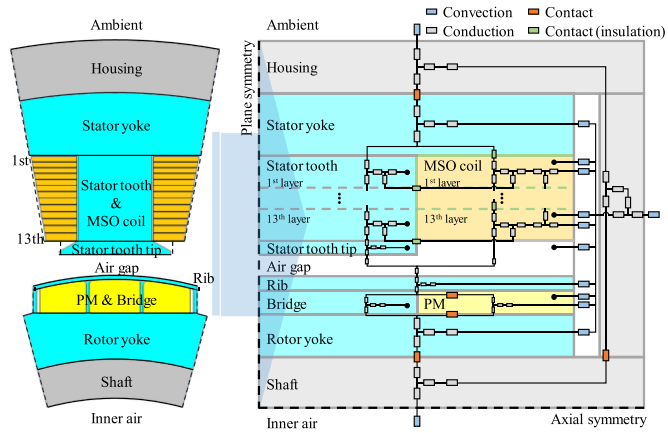

Fig. 17. Lumped parameter thermal network of PMSM using MSO coil.

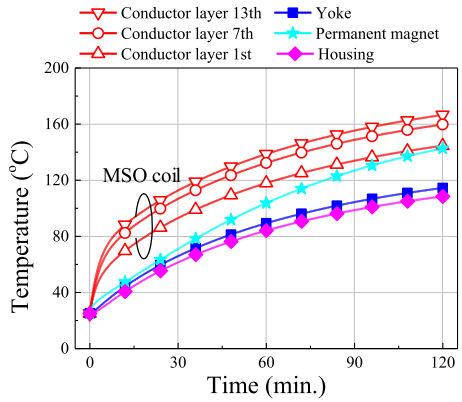

Fig. 18. Thermal analysis result of improved model (1600RPM, 67.5kW).

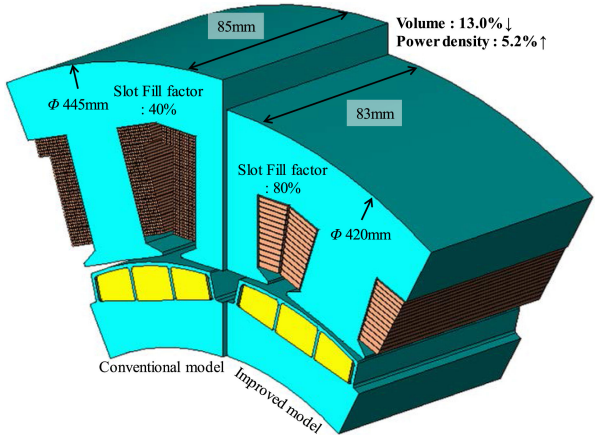

Fig. 19. Comparison between conventional model and improved model.

because of a large filled area of insulation coating between each conductor, and it also deteriorates the heat dissipation rate. However, the MSO coil has a large contact area with the stator core and with each conductor. Also, owing to its small filled area of insultation coating, MSO coil has high slot fill factor. As a result, MSO coil has a great dissipation rate of heat due to reasons commented above.

TABLE V
COMPARISON BETWEEN CONVENTIONAL MODEL AND IMPROVED MODEL

Item	Unit	Conventional model	Improved model
Pole / Slot	-	12 / 18	
Current density	A_{rms}/mm^2	11	
Series turns per phase	-	39	
Number of parallel circuits	-	2	
Slot fill factor	%	40	80
Stator diameter / Stack length	mm	445/85	420/83
Volume (Without housing)	m^3	0.0132	0.0115
Split ratio	-	0.66	0.72
Torque density	kNm/m^3	60.5	69.6
Power density	kW/kg	1.91	2.01

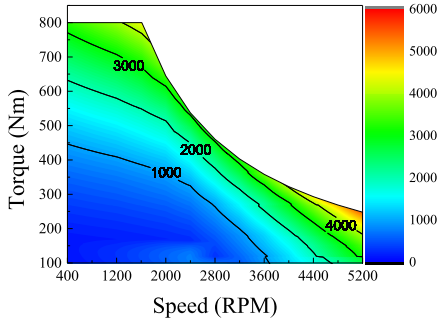

Fig. 20. Simulation result of AC loss for improved model.

To analyze the thermal characteristics of PMSM rigorously, the thermal analysis is conducted by the lumped parameter thermal network (LPTN), which is one of the most widely used method for thermal analysis [35]–[37]. The basic principle of the proposed LPTN is based on the thermal network proposed by P. H. Mellor [35]. Considering almost all the components of the PMSM as cylindrical, the thermal resistances and capacitances are equalized as hollow cylinder shapes and calculated. Especially for MSO coil, the modeling of thermal network is based on each conductor layer so that the AC copper loss of each conductor layer can be applied to their own layer. The heat flow mechanisms of the LPTN are based on the following assumptions:

1) Radiation is ignored.
2) Only the circumferential heat flow between the stator tooth and coil is considered.
3) The thermal capacitances and heat sources are distributed uniformly in each component.

The LPTN is solved based on the linear differential equation (7) for all nodes:

$$C_i \frac{dT_i}{dt} = \frac{1}{R_{ji}} (T_j - T_i) + \dot{Q}_i \tag{7}$$

where, C_i is the thermal capacitance of the node, T_i and T_j are the ith and jth node temperatures, respectively, R_{ji} is the thermal resistance between the two adjacent nodes i and j, and $\dot{Q}_i$ is the heat flow rate at node i, which is the loss.

For convection in electric motors, the thermal convection resistance is related to not only the dimension but also the state

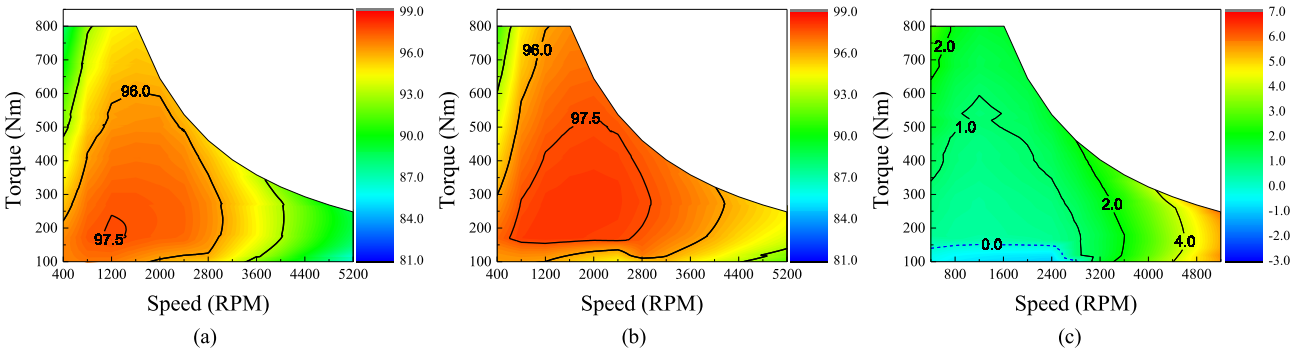

Fig. 21. Efficiency map. (a) Conventional model. (b) Improved model. (c) Difference of efficiency between conventional model and improved model.

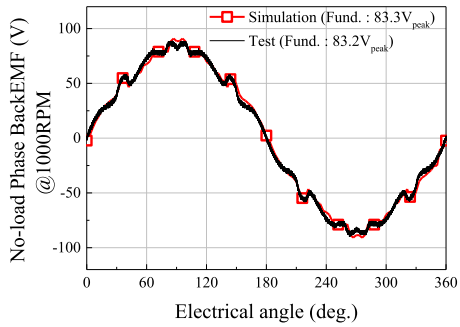

Fig. 22. No-load phase back electromotive force @ 1000RPM.

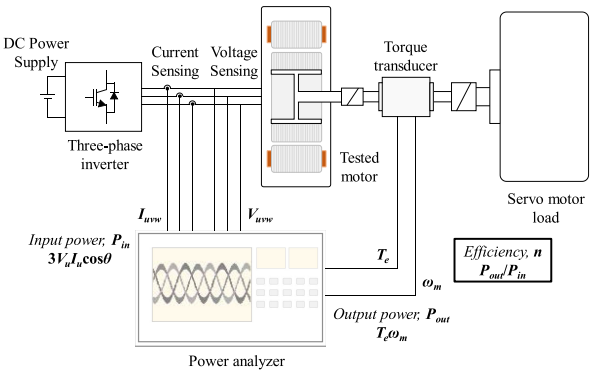

Fig. 23. Diagram of load test to measure efficiency.

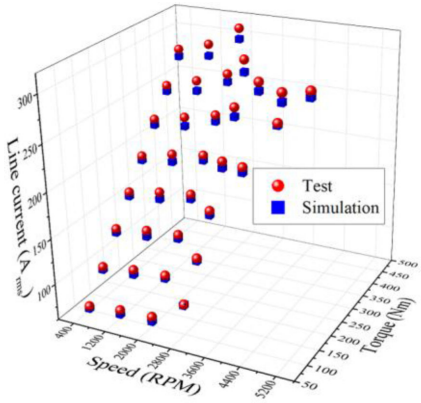

Fig. 24. Comparison of simulation and test result for line current.

of the air flow. The following three cases of convection are considered:

1) Frame-ambient
2) Air gap: stator–rotor
3) Air between end cover and stator, and end cover and rotor

The convection heat transfer coefficients in these cases are decided by the empirical equations investigated beforehand [38]–[40]. Moreover, the contact states between different materials are applied as contact heat transfer resistances and their contact thermal coefficients are also determined by the empirical equations studied earlier [41].

Lastly, the losses such as AC copper loss, iron loss, and PM eddy current loss are obtained by FEA and the mechanical loss is obtained from the previous Section. As aforementioned, the AC copper loss of each conductor layer is accessed by FEA and is applied as heat source in each conductor layer in LPTN. Consequently, the configured LPTN for PMSM using MSO coil is shown in Fig. 17 and the thermal analysis result of improved model at the condition of base speed and half maximum output power (1600RPM, 67.5kW) is shown in Fig. 18. The result shows that the heat dissipation from the MSO coil of the improved model is good enough to be used over the insulation class of H for 2 hours of operation, having the maximum operating temperature up to 180° C. However, the improved model needs some effort to improve the heat dissipation from rotor, especially for permanent magnet.

V. Result and Verification

A. Performance of Improved Model

The improved model with an MSO coil was chosen by selecting the pole/slot number of 12/18, current density of 11 A_{rms}/mm^2, and number of parallel circuits as 2. Fig. 19 shows the shape of conventional and improved models exhibiting a 5.2% increase in power density and a 13% decrease in volume without the housing, compared to the conventional model. Table V shows the improved model parameters compared with the conventional model. When conducting FEA with conventional

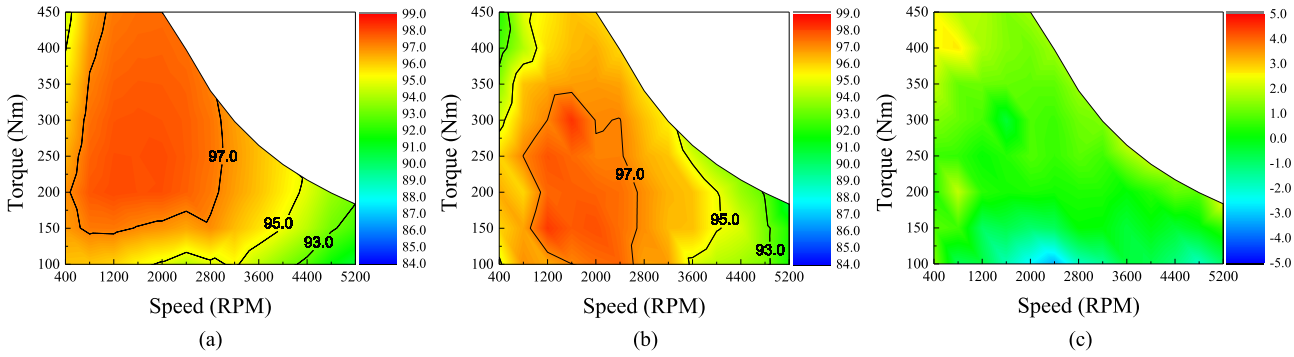

Fig. 25. Efficiency map verification of improved model. (a) Simulation result. (b) Test result. (c) Difference of efficiency between simulation and test results.

model, the transposition of strands is not applied. From the FEA result, the simulated AC loss results for the improved model are shown in Fig. 20. Finally, Fig. 21 presents the efficiency maps and their differences, showing higher efficiency for the improved model compared to the conventional model in almost all driving ranges, except for low speed and low torque.

B. Verification

Before verifying the simulation results of the improved model with the load test, the back electromotive force (BEMF) was measured to compare with the simulation results by conducting a no-load test and the result is shown in Fig. 22. It can be seen that the specimen was properly manufactured because the fundamental BEMF error between the experiment and simulation results was 1.2%.

To verify the proposed study's validity in this paper, the load test to obtain an efficiency map of the improved model was conducted. Fig. 15 shows the experimental setup for the load test. The improved model, HBM T40B torque transducer, and servo motor are connected in series. As the peak torque capability of the torque transducer was 450 Nm, the maximum power was limited to 100 kW in the experiments. The improved model was driven by the motor drive with an embedded Texas Instruments TMS320F28335 digital signal processor, and the current control loop was operated at 12 kHz. The Yokogawa WT3000 power analyzer was used for calculating the efficiency of the improved model. For calculating the efficiency, line-line voltages and line currents were measured using the voltage and current probe, and the load torque and rotating speed were measured using a torque transducer as shown in Fig. 23.

The load test was performed with a power range of up to 100 kW and a speed of up to 5200 RPM. Fig. 24 shows simulation and test results of the line current applied to the improved model. The line current trends for simulation and test fit well along the entire range of speed and torque. Owing to additional losses from current harmonics such as chopping frequency, the line currents of test are slightly larger than that of the simulation for all speed-torque ranges. Therefore, the simulation and test efficiency maps presented in Fig. 25 exhibited good compliance, with a difference within 2%p.

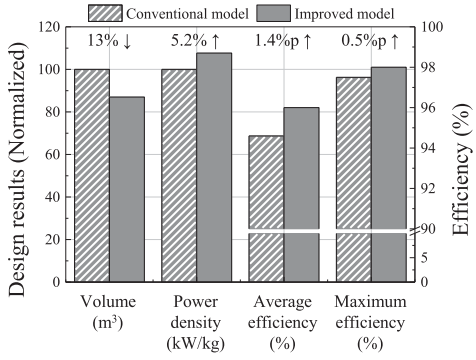

Fig. 26. Design results.

Consequently, the proposed investigation is effective regarding size, power density, and efficiency, as shown in Fig. 26. The improved model reduced the volume size by 13%, and improved power density by 5.2% compared to the conventional model. The average and maximum efficiencies were improved by 1.4%p and 0.5%p, respectively.

VI. Conclusion

In this work, a high-efficiency PMSM for EV traction was studied with a high slot fill factor coil, named an MSO coil. Due to the possible efficiency degradation due to AC copper loss of the MSO coil, the PMSM for EV traction was investigated by reducing the AC resistance of the MSO coil. Prior to this study, parameters affecting the AC resistance of the MSO coil were identified. The pole/slot numbers, current density and number of parallel circuits were determined as variables from their relation to parameters such as frequency, conductor height, width, and number of conductor layers, which critically affect AC resistance. Then, the AC resistance trend was analyzed by the proposed analytical method and FEA was performed to calculate the AC resistance, according to the above variables.

Based on the results, the pole/slot numbers, current density, and number of parallel circuits were decided as 12p/18s, 11 A_{rms}/mm^2, and 2, respectively, to reduce the AC resistance. Compared to the conventional model using round wire, the

improved model with an MSO coil showed 13% smaller volume, 5.2% higher power density, and higher overall efficiency. Finally, the improved model was manufactured and an efficiency test was conducted. Test results showed a tendency similar to simulation results in almost all driving range, with errors mostly within 1–2%p.

REFERENCES

[1] J. de Santiago *et al.*, "Electrical motor drivelines in commercial all-electric vehicles: A review," *IEEE Trans. Veh. Technol.*, vol. 61, no. 2, pp. 475–484, Feb. 2012.

[2] K. T. Chau, C. C. Chan, and C. Liu, "Overview of permanent-magnet brushless drives for electric and hybrid electric vehicles," *IEEE Trans. Ind. Electron.*, vol. 55, no. 6, pp. 2246–2257, Jun. 2008.

[3] J. Wang, X. Yuan, and K. Atallah, "Design optimization of a surface-mounted permanent-magnet motor with concentrated windings for electric vehicle applications," *IEEE Trans. Veh. Technol.*, vol. 62, no. 3, pp. 1053–1064, Mar. 2013.

[4] V. Ruuskanen, J. Nerg, J. Pyrhönen, S. Ruotsalainen, and R. Kennel, "Drive cycle analysis of a permanent-magnet traction motor based on magnetostatic finite-element analysis," *IEEE Trans. Veh. Technol.*, vol. 64, no. 3, pp. 1249–1254, Mar. 2015.

[5] C. Du-Bar and O. Wallmark, "Eddy current losses in a hairpin winding for an automotive application," in *Proc. 23th ICEM*, Alexandroupoli, Greece, Sep. 2018, pp. 710–716.

[6] G. Berardi and N. Bianchi, "Design guideline of an AC hairpin winding," in *Proc. 23th ICEM*, Alexandroupoli, Greece, Sep. 2018, pp. 2444–2450.

[7] H. J. Park and M. S. Lim, "Design of high power density and high efficiency wound-field synchronous motor for electric vehicle traction," *IEEE Access*, vol. 7, pp. 46677–46685, 2019.

[8] H. Akita, Y. Nakahara, N. Miyake, and T. Oikawa, "New core structure and manufacturing method for high efficiency of permanent magnet motors," in *Proc. Conf. Rec. IEEE Ind. Appl. Annu. Meeting*, Salt Lake, UT, USA, Oct. 2003, vol. 2, pp. 367–372.

[9] H. Huang and L. Chang, "Electrical two-speed propulsion by motor winding switching and its control strategies for electric vehicles," *IEEE Trans. Veh. Technol.*, vol. 48, no. 2, pp. 607–618, Mar. 1999.

[10] M. S. Lim and J. P. Hong, "Design of high efficiency wound field synchronous machine with winding connection change method," *IEEE Trans. Energy. Convers.*, vol. 33, no. 4, pp. 1978–1987, Dec. 2018.

[11] M. S. Lim, S. H. Chai, and J. P. Hong, "Design of saliency-based sensorless-controlled IPMSM with concentrated winding for EV traction," *IEEE Trans. Magn.*, vol. 52, no. 3, Mar. 2016, Art. no. 8110004.

[12] M. Paradkar and J. Böcker, "Analysis of Eddy current losses in the stator windings of IPM machines in electric and hybrid electric vehicle applications," in *Proc. 8th PEMD*, Apr. 2016, pp. 1–5.

[13] I. Petrov, M. Polikarpova, P. Ponomarev, P. Lindh, and J. Pyrhönen, "Investigation of additional AC losses in tooth-coil winding PMSM with high electrical frequency," in *Proc. 22th ICEM*, Lausanne, Switzerland, Sep. 2016, pp. 1841–1846.

[14] J. Chin, K. Cha, E. Lee, S. Park, J. Hong, and M. Lim, "Design of PMSM for EV traction using MSO coil considering AC resistance according to current density and parallel circuit," in *Proc. IEEE Veh. Power Propulsion Conf.*, Hanoi, Vietnam, 2019, pp. 1–6.

[15] K. Cha, J. Chin, E. Lee, S. Park, J. Hong, and M. Lim, "AC resistance reduction design of traction motor for high energy efficiency of electric vehicle," in *Proc. IEEE Veh. Power Propulsion Conf.*, Hanoi, Vietnam, 2019, pp. 1–6.

[16] E. C. Lee, S. O. Kwon, H. Y. Lee, S. W. Lee, and K. W. Lee, "Method for manufacturing MSO COIL and device for manufacturing same," U.S. Patent 20200099279, Mar. 26, 2020.

[17] T. Gillespie, *Fundamentals of Vehicle Dynamics*, 2nd ed., SAE, 2020.

[18] D. Kim, P. Benoliel, D. Kim, T. H. Lee, J. W. Park, and J. Hong, "Framework development of series hybrid powertrain design for heavy-duty vehicle considering driving conditions," *IEEE Trans. Veh. Technol.*, vol. 68, no. 7, pp. 6468–6480, Jul. 2019.

[19] K. S. Cha, D. M. Kim, Y. H. Jung, and M. S. Lim, "Wound field synchronous motor with hybrid circuit for neighborhood electric vehicle traction improving fuel economy," *Appl. Energy*, vol. 263, 2020, Art. no. 114618.

[20] J. Pyrhönen, T. Jokinen, and V. Hrabovcová, in *Design of Rotating Electrical Machines*, 2nd ed., NY, NY, USA: John Wiley Sons, 2013.

[21] Z. Yang, F. Shang, I. P. Brown, and M. Krishnamurthy, "Comparative study of interior permanent magnet, induction, and switched reluctance motor drives for EV and HEV applications," *IEEE Trans.Transp. Elect*, vol. 1, no. 3, pp. 245–254, Oct. 2015.

[22] M. Popescu, J. Goss, D. A. Staton, D. Hawkins, Y. C. Chong, and A. Boglietti, "Electrical vehicles—Practical solutions for power traction motor systems," *IEEE Trans. Ind. Appl.*, vol. 54, no. 3, pp. 2751–2762, May/Jun. 2018.

[23] A. Tessarolo, C. Ciriani, M. Bortolozzi, M. Mezzarobba, and N. Barbini, "Investigation into multi-layer fractional-slot concentrated windings with unconventional slot-pole combinations," *IEEE Trans. Energy Convers.*, vol. 34, no. 4, pp. 1985–1996, Dec. 2019.

[24] G. Dajaku, W. Xie, and D. Gerling, "Reduction of low space harmonics for the fractional slot concentrated windings using a novel stator design," *IEEE Trans. Magn.*, vol. 50, no. 5, May 2014, Art. no. 8201012.

[25] L. Alberti, E. Fornasiero, and N. Bianchi, "Impact of the rotor yoke geometry on rotor losses in permanent-magnet machines," *IEEE Trans. Ind. Appl.*, vol. 48, no. 1, pp. 98–105, Jan./Feb. 2012.

[26] H. Yang and Y. Chen, "Influence of radial force harmonics with low mode number on electromagnetic vibration of PMSM," *IEEE Trans. Energy Convers.*, vol. 29, no. 1, pp. 38–45, Mar. 2014.

[27] S. G. Min and B. Sarlioglu, "Modeling and investigation on electromagnetic noise in PM motors with single- and double-layer concentrated winding for EV and HEV application," *IEEE Trans. Transp. Electrific.*, vol. 4, no. 1, pp. 292–302, Mar. 2018.

[28] M. Park, J. Jung, D. Kim, J. Hong, and M. Lim, "Design of high torque density multi-core concentrated flux-type synchronous motors considering vibration characteristics," *IEEE Trans. Ind. Appl.*, vol. 55, no. 2, pp. 1351–1359, Mar./Apr. 2019.

[29] Y. Jung, M. Lim, M. Yoon, J. Jeong, and J. Hong, "Torque ripple reduction of IPMSM applying asymmetric rotor shape under certain load condition," *IEEE Trans. Energy Convers.*, vol. 33, no. 1, pp. 333–340, Mar. 2018.

[30] T. Arakawa *et al.*, "Examination of an interior permanent magnet type axial gap motor for the hybrid electric vehicle," *IEEE Trans. Magn.*, vol. 47, no. 10, pp. 3602–3605, Oct. 2011.

[31] R. Wrobel, P. Mellor, M. Popescu, and D. Staton, "Power loss analysis in thermal design of permanent magnet machines – a review," *IEEE Trans. Ind. Appl.*, vol. 52, no. 2, pp. 1359–1368, Mar/Apr. 2015.

[32] J. Chin, S. Hwang, H. Park, and J. Hong, "Thermal analysis and verification of PMSM using LPTN considering mechanical components and losses," in *Proc. 23th ICEM*, Alexandroupoli, Greece, Sep. 2018, pp. 1323–1329.

[33] R. Wrobel, G. Vainel, C. Copeland, T. Duda, D. Staton, and P. H. Mellor, "Investigation of mechanical loss components and heat transfer in an axial-flux PM machine," *IEEE Trans. Ind. Appl.*, vol. 51, no. 4, pp. 3000–3011, Jul./Aug. 2015.

[34] T. A. Harris and M. N. Kotzalas, in *Advanced Concepts of Bearing Technology—Rolling Bearing Analysis*. Boca Raton, FL, USA: CRC Press., 2007.

[35] P. H. Mellor, D. Roberts, and D. R. Turner, "Lumped parameter thermal model for electrical machines of TEFC design," *IEE Proc. B Elect. Power Appl.*, vol. 138, no. 5, pp. 205, 1991.

[36] A. Boglietti, A. Cavagnino, D. Staton, M. Shannel, M. Mueller, and C. Mejuto, "Evolution and modern approaches for thermal analysis of electrical machines," *IEEE Trans. Ind. Electron.*, vol. 56, no. 3, pp. 871–882, Mar. 2009.

[37] A. Tessarolo and C. Bruzzese, "Computationally efficient thermal analysis of a low-speed high-thrust linear electric actuator with a three-dimensional thermal network approach," *IEEE Trans. Ind. Electron.*, vol. 62, no. 3, pp. 1410–1420, Mar. 2015.

[38] D. Staton, A. Boglietti, and A. Cavagnino, "Solving the more difficult aspects of electric motor thermal analysis in small and medium size industrial induction motors," *IEEE Trans. Energy Convers.*, vol. 20, no. 3, pp. 620–628, Sep. 2005.

[39] J. Nerg, M. Rilla, and J. Pyrhönen, "Thermal analysis of radial-flux electrical machines with a high power density," *IEEE Trans. Ind. Electron.*, vol. 55, no. 10, pp. 3543–3554, Oct. 2008.

[40] D. A. Staton and A. Cavagnino, "Convection heat transfer and flow calculations suitable for electric machines thermal models," *IEEE Trans. Ind. Electron.*, vol. 55, no. 10, pp. 3509–3516, Oct. 2008.

[41] R. Camilleri, D. A. Howey, and M. D. McCulloch, "Experimental investigation of the thermal contact resistance in shrink fit assemblies with relevance to electrical machines," in *Proc. 7th IET Int. Conf. Power Electron., Mach. Drives*, 2014, pp. 1–9.

Jun-Woo Chin received the bachelor's degree in mechanical engineering from Hanyang University, Seoul, South Korea, in 2014. He is currently working toward the Ph.D. degree in automotive engineering from Hanyang University. His research interests are the design of electric machines for automotive, losses and thermal analysis of electric motor and generator.

Kyoung-Soo Cha received the bachelor's degree in electric engineering from Chungbuk University, South Korea in 2015. He is currently working toward the Ph.D. degree in automotive engineering from Hanyang University, South Korea. His research interests are electric machine design for automotive, home appliance, and rare-earth free machine.

Min-Ro Park received the bachelor's degree in electrical engineering from Chungnam National University, Daejeon, South Korea, in 2013, and the integrated master's and Ph.D. degrees in automotive engineering from Hanyang University, Seoul, South Korea, in 2020. Since 2020, he has been with Korea Institute of Robotics and Technology Convergence (KIRO), Pohang, South Korea, where he is currently a Senior Researcher. His research interests include multi-physics analysis and design of electric machine for mechatronics systems.

Soo-Hwan Park received the bachelor's degree in mechanical engineering from Hanyang University, Seoul, Korea, in 2014. He is currently working toward the Ph.D. degree in automotive engineering. From 2019 to 2020, he was with the Korea Institute of Industrial Technology. His main research interests include electromagnetic field analysis, design and optimization of electric machines for automotive and robotics applications, and electric machine drive for industrial applications.

Eui-Chun Lee received the bachelor's degree in mechanical engineering from the Kumoh National Institue of Technology, South Korea in 2014,and the master's degree in mechanical engineering from Kyung-Pook National University, South Korea in 2016. He is currently working toward the Ph.D degree in automotive engineering from Hanyang University, South Korea. Since 2019, he has been with the Korea Institue of Industrial Technology (KITECH), where he is currently a Researcher with Mechatronics Convergence Research Group. His main research field include HEV, EV, Robot, Drone Drive Motor Design and Productive Electric Machine Manufacturing Process.

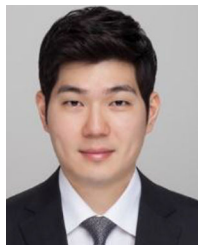

Myung-Seop Lim (Member, IEEE) received the bachelor's degree in mechanical engineering and the master's and the Ph.D. degrees in automotive engineering from Hanyang University, Seoul, South Korea, in 2012, 2014 and 2017, respectively.

From 2017 to 2018, he was a Research Engineer with Hyundai Mobis, Yongin, South Korea. From 2018 to 2019, he was an Assistance Professor with Yeungnam University, Daegu, South Korea, Since 2019, he has been with Hanyang University, Seoul, South Korea, where he is currently an Assistant Professor.

His research interests include electromagnetic field analysis and multi-physics analysis of electric machinery for mechatronics systems such as automotive and robot applications.